

Lepton Collider as a window to Reheating

Basabendu Barman*

Department of Physics, School of Engineering and Sciences, SRM University-AP, Amaravati 522240, India

Subhaditya Bhattacharya,[†] Sahabub Jahedi,[‡] Dipankar Pradhan,[§] and Abhik Sarkar[¶]
Department of Physics, Indian Institute of Technology, Guwahati, Assam-781039, India

We propose a search strategy for MeV-scale feebly interacting massive particle (FIMP) dark matter (DM) at the e^+e^- collider. We argue, detection of a mono- γ signal plus missing energy can indicate to an MeV-scale reheating temperature of the Universe, after addressing observed DM abundance and other relevant constraints.

High energy particle colliders are essential tools for new physics (NP) search, where we supposedly recreate Universe at high temperature, close to the Big Bang. Our study attempts to address whether a correspondence can be established between collider signal and the early Universe cosmology, focusing particularly on the pre-Big Bang Nucleosynthesis (BBN) epoch.

The cosmology of the early Universe has a profound impact on the production of exotic relics, for example, the Dark Matter (DM), that constitutes about 26% of the matter-energy budget of the Universe [1]. Many questions revolve around DM: what is its fundamental nature, what is the production mechanism, or, how to possibly detect such entities. A particle DM is well motivated to fit the observations, having any intrinsic spin, minimal photon coupling, and stable of the order of Universe's life time. Depending on whether they were produced in equilibrium with the thermal bath or not, they are largely classified as weakly interacting massive particles (WIMPs) [2] and feebly interacting massive particles (FIMPs) [3].

FIMPs having feeble interaction with the visible Universe, can be produced from out-of-equilibrium decay or scattering of the SM particles and can easily evade stringent experimental bounds, unlike WIMPs. In a typical UV freeze-in [4], DM number density becomes proportional to the temperature of the thermal bath. Thus bulk of the DM is produced at the highest temperature of the Universe, usually known as the reheating temperature, when reheating happens instantaneously. The crucial point is, since freeze-in occurs out of equilibrium, DM retains the “memory” of the early Universe cosmology. Detecting such relics at the colliders could therefore provide a probe of the reheating temperature or early Universe cosmology.

Effective Field Theory (EFT) approach [5–9] to search for DM is economic in terms of the number of independent

parameters and efficient in capturing the essential characteristics of a physical phenomenon, focusing solely on the relevant degrees of freedom present at a certain scale. EFT methodologies are widely used, including condensed matter systems (see, [10]), and have emerged as a standard prescription for studying physics beyond the SM, but limited, if collider experiments reveal a direct manifestation of the heavy mediator, generating the effective interactions. EFT is therefore valid when the center-of-mass (CM) energy of the collision remains lower than the heavy mediator mass. This is easier to achieve in lepton colliders than the hadronic ones, since the partonic CM energy differs from the exact CM energy in the latter case.

At collider, as DM evades detection, the visible particles produced from the initial state radiation (ISR) or in association with DM can provide vital clues via momentum or energy imbalance to search for DM. Mono- X , ($X \in \gamma, j, Z, H$) plus missing energy (\cancel{E}) final state is one of the popular probes to search for DM at colliders. The signal of our interest is mono- γ , which has been studied widely at the lepton colliders [11–24]. Noticeably, this final state with ISR photon has similar \cancel{E} event distribution to the huge SM neutrino background ($\nu\bar{\nu}\gamma$), making it difficult for signal-background separation (see supplemental material). This motivates us to look for associate photon production, which we call *natural* mono- γ signal within the EFT framework.

Dimension-six and seven EFT operators with real scalar (Φ) and fermionic (χ) DM leading to natural mono-photon searches are,

$$\mathcal{O}_2^s : \frac{c_\Phi}{\Lambda^2} (B_{\mu\nu} B^{\mu\nu} + W_{\mu\nu}^i W^{i\mu\nu}) \Phi^2, \quad (1)$$

$$\mathcal{O}_3^f : \frac{c_\chi}{\Lambda^3} (B_{\mu\nu} B^{\mu\nu} + W_{\mu\nu}^i W^{i\mu\nu}) (\bar{\chi}\chi), \quad (2)$$

where $W_{\mu\nu}^i$ ($i = 1, 2, 3$) and $B_{\mu\nu}$ are the electroweak field strength tensors corresponding to $SU(2)_L$ and $U(1)_Y$ respectively, and $c_{\Phi, \chi}$ are the dimensionless Wilson-coefficients¹. The presence of DM fields in pair implies

* basabendu.b@srmap.edu.in

† subhab@iitg.ac.in

‡ sahabub@iitg.ac.in

§ d.pradhan@iitg.ac.in

¶ sarkar.abhik@iitg.ac.in

¹ It is straightforward to extend the operators involving complex

Z_2 -symmetry that ensures absolute stability of the DM. These operators are well-studied in the context of freeze-out, with a primary focus to constrain direct and indirect searches, complementing the LHC search bounds [25–27]. For a UV complete model, see supplementary material. We however discuss DM production via freeze-in and derive the viable parameter space that complies with the observed DM abundance. The essential feature of freeze-in production is to consider that the DM number density was vanishingly small in the early Universe, then produced dynamically from the visible sector via DM-SM interactions, $\gamma\gamma \rightarrow \text{DM DM}$ in our case, emerging from Eq. (1) and (2). The DM-SM interaction strength, however, is several orders of magnitude feeble than the weak interaction strength, such that the DM stays out of equilibrium. The limiting condition can be estimated by comparing the DM interaction rate $\Gamma_{2\rightarrow 2} = n_{\text{DM}}^{\text{eq}} \langle \sigma v \rangle_{\gamma\gamma \rightarrow \text{DM, DM}}$ with the Hubble rate H , where $\langle \sigma v \rangle$ is the thermally averaged DM production cross-section [28], so that,

$$\frac{\Gamma_{2\rightarrow 2}}{H} \Big|_{T=m_{\text{DM}}} \simeq \frac{M_P}{\sqrt{g_*(T)}} \times \begin{cases} \mathcal{C}_0 \left(\frac{m_\Phi}{1\text{MeV}}\right)^3 \left(\frac{1\text{TeV}}{\Lambda}\right)^4 & \text{for scalar,} \\ \mathcal{C}_{1/2} \left(\frac{m_\chi}{1\text{MeV}}\right)^5 \left(\frac{1\text{TeV}}{\Lambda}\right)^6 & \text{for fermion.} \end{cases} \quad (3)$$

Here, $\mathcal{C}_0 \simeq 7 \times 10^{-3}$ and $\mathcal{C}_{1/2} \simeq 2.7 \times 10^{-14}$, achieved by a conservative estimate of assuming DM number density to be the same as the equilibrium number density, i.e. $n_{\text{DM}} \equiv n_{\text{DM}}^{\text{eq}} = T/(2\pi^2) m_{\text{DM}}^2 K_2(m_{\text{DM}}/T)$. As one can infer, it is easy to satisfy the out-of-equilibrium condition for fermionic DM compared to the scalar case due to larger suppression. The very idea that we wish to investigate the collider signature of freeze-in, drives us to choose $\Lambda \sim \mathcal{O}(\text{TeV})$ such that the collider signal is significant enough, which in turn demands $m_{\text{DM}} \sim \mathcal{O}(\text{MeV})$ to avoid overclosing the Universe.

Because of the non-renormalizable nature of the interaction, we see, DM yield features the typical UV nature [4] (see supplementary material), where bulk of the DM is produced around the highest temperature. When the inflaton decays *instantaneously*, maximum temperature (T_{max}) achieved by the thermal bath corresponds to the reheat temperature T_{RH} ², and is given by

$$T_{\text{RH}} = \left(\frac{90}{\pi^2 g_*}\right)^{1/4} \sqrt{\Gamma_\phi M_P}, \quad (4)$$

scalar and vector DM leading to natural mono- γ , however we aim to address them in an accompanying paper.

² The temperature of the Universe, however, can be several orders of magnitude larger than T_{RH} [29].

where Γ_ϕ is the total inflaton (ϕ) decay width to radiation. Note that, Eq. (4) also indicates the onset of radiation domination. We, however, remain agnostic about the reheating mechanism (and inflaton decay modes). For DM production via $\gamma\gamma \rightarrow \text{DM DM}$ channel, an approximate analytical expression for DM yield $Y = n/s$ can be obtained by solving the corresponding Boltzmann equation (BEQ) (see supplemental material)

$$Y_{\text{DM}}(T) = \frac{270 \sqrt{10} M_P}{g_{*s}(T) \sqrt{g_*(T)} \pi^8} \begin{cases} c_\Phi^2 \frac{T_{\text{RH}}^3 - T^3}{\Lambda^4} & \text{for scalar,} \\ c_\chi^2 \frac{288}{5} \frac{T_{\text{RH}}^5 - T^5}{\Lambda^6} & \text{for fermion,} \end{cases} \quad (5)$$

considering $s \gg 4 m_{\text{DM}}^2$. To fit the observed DM relic density, $Y_0 m_{\text{DM}} = \Omega h^2 \frac{1}{s_0} \frac{\rho_c}{h^2} \simeq 4.3 \times 10^{-10} \text{ GeV}$, where Y_0 , is the present day yield. Here $\rho_c \simeq 1.05 \times 10^{-5} h^2 \text{ GeV/cm}^3$ is the critical energy density, $s_0 \simeq 2.69 \times 10^3 \text{ cm}^{-3}$ the present entropy density [30], and $\Omega h^2 \simeq 0.12$ is the observed abundance of DM relics [1]. From Eq. (5), it is clear that, for a given DM mass and effective scale, the yield is maximum at $T_{\text{RH}} \gg T$, which is the quintessential feature of UV freeze-in. The DM abundance is governed by four independent parameters: $\{c_{\Phi, \chi}, m_{\text{DM}}, T_{\text{RH}}, \Lambda\}$, although we assume $c_{\Phi, \chi} = 1$ for simplification. The effective description of Eq. (1) and (2) remains valid under the hierarchy: $\Lambda > T_{\text{RH}} \gtrsim m_{\text{DM}}$, implying, the cut-off scale Λ stands as the highest scale of the theory. In case of instantaneous decay approximation, maximum mass for the DM produced from the thermal bath can be $m_{\text{DM}} \simeq T_{\text{RH}}$ ³. In order to produce the observed DM abundance, using eq. (5) we find

$$\Lambda \simeq \begin{cases} 5 \text{ TeV} \left(\frac{m_\Phi}{1\text{MeV}}\right)^{1/4} \left(\frac{T_{\text{RH}}}{T_{\text{BBN}}}\right)^{3/4} & \text{for scalar,} \\ 100 \text{ GeV} \left(\frac{m_\chi}{1\text{MeV}}\right)^{1/6} \left(\frac{T_{\text{RH}}}{T_{\text{BBN}}}\right)^{5/6} & \text{for fermion,} \end{cases} \quad (6)$$

which shows, in order to have $\Lambda \simeq \mathcal{O}(\text{TeV})$, we need to opt for low DM mass, as well as low T_{RH} . It is easier to achieve for \mathcal{O}_3^f , because of larger suppression. Note $T_{\text{BBN}} \simeq 4 \text{ MeV}$ [33] corresponds to the lower bound on T_{RH} , such that the accurate measurement of light element abundance during BBN is not hampered. This order of magnitude estimation conforms well with the full numerical results as illustrated in Fig. 1, showing relic density allowed parameter space in $T_{\text{RH}} - m_{\text{DM}}$ plane, where different shades of bands correspond to different values of Λ . Interestingly, 5σ significance for the mono- $\gamma + \cancel{E}$ signal produced by the DM at the ILC (with $\sqrt{s} = 1 \text{ TeV}$, and

³ For inflaton decaying with finite width, it is also possible to produce DM *during* reheating with $T_{\text{max}} < m_{\text{DM}} \lesssim T_{\text{RH}}$ [31, 32].

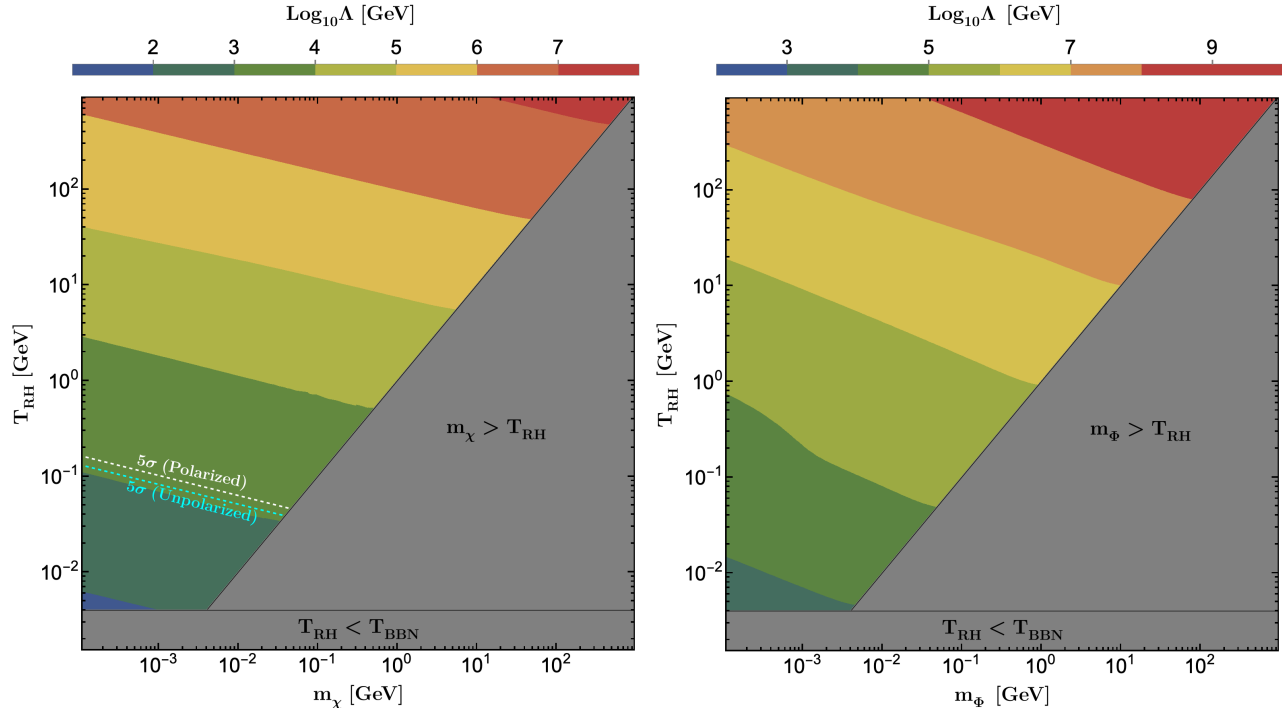


FIG. 1. DM relic allowed parameter space for fermion (left) and scalar (right), where the colour bar corresponds to Λ . The gray shaded regions are disallowed from instantaneous decay approximation that requires $m_{\text{DM}} \lesssim T_{\text{RH}}$, as well as from BBN bound on $T_{\text{RH}} \gtrsim 4$ MeV. In the left panel the cyan and white dashed contours shows 5σ significance for mono- $\gamma + \cancel{E}$ signal at the ILC, with $\sqrt{s} = 1$ TeV, and $\mathcal{L}_{\text{int}} = 8 \text{ ab}^{-1}$ for unpolarized and polarized ($\{P_{e^+}, P_{e^-}\} = \{-20\%, +80\%\}$) cases, respectively.

integrated luminosity $\mathcal{L}_{\text{int}} = 8 \text{ ab}^{-1}$) can be projected in this plane, as shown by the (cyan) white dashed lines for (un)polarized beams in the left panel plot, indicating the possibility of collider reach to probe the MeV-scale reheating era. We elaborate on it soon.

It is worth reminding that MeV-scale reheating is realizable in minimal gravitational reheating scenario, where the SM bath is produced from inflaton scattering, mediated by graviton [34]. Since gravity interacts with all matter particles democratically, such a reheating process is inevitable and natural. The minimal scenario is however dismissed due to the excessive production of inflationary gravitational wave energy density around the time of BBN [35, 36]. As mentioned before, we refrain from adhering to a specific reheating mechanism here, and simply consider T_{RH} as a free parameter.

The photophilic DM having $\gamma\gamma$ -DM,DM interaction, provides mono- γ with missing energy signal as the innate choice, as shown in the left panel of Fig. 2. For collider simulation we consider \mathcal{O}_3^f , since for \mathcal{O}_2^s , one needs $T_{\text{RH}} < T_{\text{BBN}}$ in order to have $\Lambda \lesssim \mathcal{O}(\text{TeV})$, as seen from Fig. 1. For larger Λ , the signal significance diminishes as the production cross-section reduces. We perform detector-level analysis at the projected $\sqrt{s} = 1$ TeV and $\mathcal{L}_{\text{int}} = 8 \text{ ab}^{-1}$ which is expected to be the maximum reach of the ILC [37]. The model implementation is done

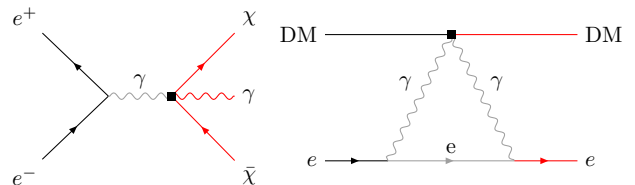


FIG. 2. *Left*: Feynman graph for associated production of fermionic DM pair ($\chi\bar{\chi}$) with mono- γ at the e^+e^- collider. *Right*: Feynman diagram corresponds to the FIMP-electron (DM - e) scattering.

in `FeynRules` [38] and the signal/background events are generated using `MG5_aMC` [39]. The simulated events are then showered using `Pythia8` [40] and further detector simulation is done exploiting `Delphes3` [41].

The signal selection is ensured by only allowing events with a single photon with no associated leptons or jets. The dominant SM background stems from $\nu\bar{\nu}\gamma$ channel, where the photon can be radiated from the electron leg in the W mediated t -channel (dominant), Z mediated s -channel or from the W boson fusion process. The photon from the SM neutrino background is characterized by low *transverse momentum* (p_T), unlike the signal. Thus, imposing *missing transverse energy* (MET),

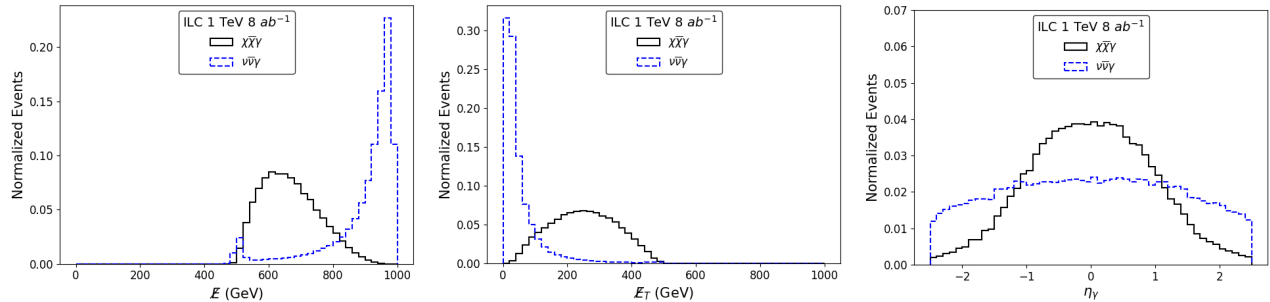


FIG. 3. *Event topology*: Signal background event distributions for different kinematic variables with the mono- γ final state signal. Left: MET (E_T), middle: ME (\cancel{E}), right: Pseudorapidity (η_γ). The signal corresponds to the benchmark: $m_\chi=33$ MeV, $\Lambda=1.14$ TeV

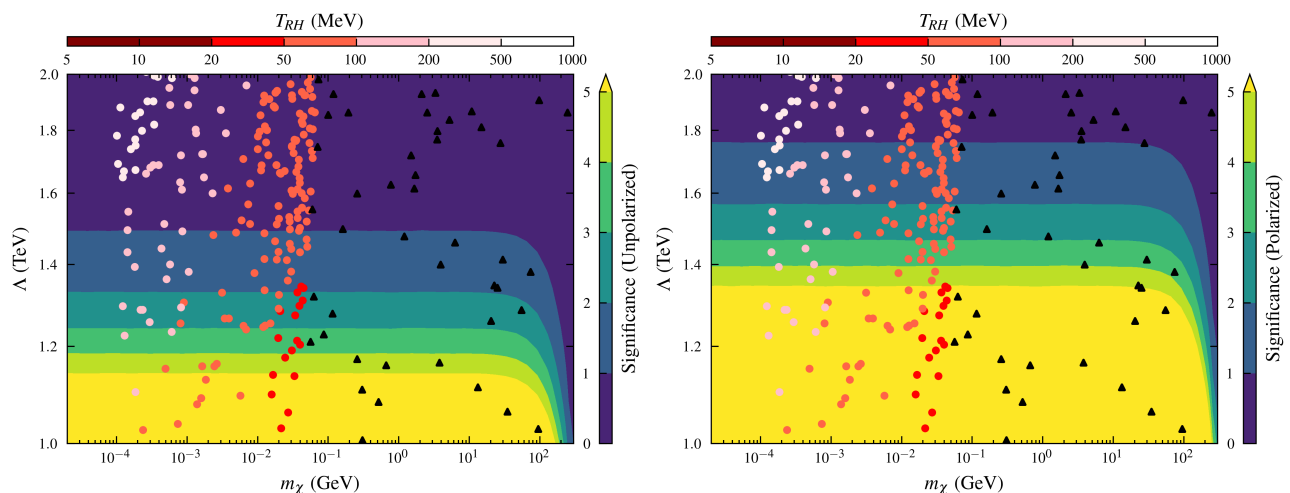


FIG. 4. *Summary plot*: The scattered red points produce observed DM abundance for fermionic DM (\mathcal{O}_3^f), for different combinations of DM mass m_χ , effective scale Λ and reheating temperature T_{RH} . The black points require $T_{RH} < T_{BBN}$ or $m_\chi > T_{RH}$ or both to produce the right abundance and, therefore, in conflict with the BBN bound, as well as instantaneous reheating approximation. The colour gradient shows the variation of signal significance for e^+e^- collider at $\sqrt{s} = 1$ TeV, and for an integrated luminosity of 8 ab^{-1} . The left panel corresponds to unpolarized incoming beam, while in the right panel, we consider polarization of $\{P_{e^+}, P_{e^-}\} = \{-20\%, +80\%\}$.

$\cancel{E}_T = -\sqrt{\sum (p_x)^2 + \sum (p_y)^2}$ (where the sum runs over all visible objects) cut effectively mitigates a substantial portion of the dominant SM background. *Missing energy* (ME) in this case is defined as $\cancel{E} = \sqrt{s} - E_\gamma$. Applying a cut to ensure the removal of the two peaks of the neutrino \cancel{E} distribution reduces the background significantly, retaining most of the signal. Finally, implementing an absolute *pseudorapidity* $|\eta_\gamma| < 1.0$ finely tunes the elimination of non-transverse backgrounds. For the benchmarks illustrated in Tab. I, the signal efficiency⁴ ϵ_s is obtained to be 0.51 for a background rejection rate of 99%. The

event topology in Fig. 3 shows the impact of these particular observables in separating the signal from the SM background. The signal significance is calculated via [42]

$$\mathcal{S} = \sqrt{2 \left[(S + B) \log \left(1 + \frac{S}{B} \right) - S \right]}. \quad (7)$$

Here S and B denote signal and background events, respectively. Signal significance (\mathcal{S}) undergoes enhancement after employing a series of cuts outlined in Tab. I. Note that, for $S/B \ll 1$, one finds $\mathcal{S} \simeq S/\sqrt{B} \propto 1/\Lambda^6$. As the SM is a left chiral theory, judicious choice of beam polarizations, as the e^+e^- machines are equipped with, can suppress the SM background, and enhance the signal significance. Owing to the proposed polarizability of ILC ($P_{e^-(e^+)} = \pm 80\%(\pm 20\%)$), we study sig-

⁴ We define $\epsilon_s = \sigma_{\text{sig}}/\sigma_{\text{prod}}$, where σ_{prod} and σ_{sig} are the signal cross-section before and after cut, respectively.

Cutflow	$\nu\bar{\nu}\gamma$ (B)	$\chi\bar{\chi}\gamma$	
		Events (S)	Significance (S)
Basic Cuts	18101325	4422	1.04
$\cancel{E}_T > 200.0$ GeV	725945	2957	3.47
$\cancel{E} \in [525, 750]$ GeV	289420	2694	5.00
$ \eta_\gamma < 1.0$	219161	2395	5.10

Polarization $\{P_{e^+}, P_{e^-}\}$	$\nu\bar{\nu}\gamma$ (B)	$\chi\bar{\chi}\gamma$	
		Events (S)	Significance (S)
$\{0\%, 0\%\}$	219161	2395	5.10
$\{+20\%, +80\%\}$	55052	2010	8.52
$\{-20\%, +80\%\}$	40711	2778	13.62
$\{+20\%, -80\%\}$	453639	2774	4.11
$\{-20\%, -80\%\}$	303079	2003	3.63

TABLE I. *Upper*: Signal background event counts and signal significance in each step of the subsequent cuts for mono- γ final state signal for fermion DM scenario, where $m_\chi=33$ MeV and $\Lambda=1.14$ TeV. *Lower*: Event counts and significance following the final cut for different polarization combinations.

nal significance for various choices of polarization combination at the benchmark points, as outlined in Tab. I. We observe that $\{P_{e^+}, P_{e^-}\} = \{-20\%, +80\%\}$ emerges as the most favorable combination, enhancing the signal while significantly reducing the background, while $\{P_{e^+}, P_{e^-}\} = \{-20\%, -80\%\}$ does the worst, diminishing the signal while elevating the background.

Fig. 4 shows signal significance in $\Lambda - m_\chi$ plane via coloured bands, which decreases with larger Λ , as the signal cross-section $\sim 1/\Lambda^6$. Also the significance diminishes with larger m_χ due to limited phase space. Following Eq. (5), each $\Lambda - m_\chi$ point indicate to a specific T_{RH} to satisfy the DM abundance, as shown by the reddish

points, establishing a correlation between the signal significance and T_{RH} . For higher DM masses, a lower T_{RH} is required to achieve the correct DM relic, which violates the lower bound on T_{RH} from BBN or the instantaneous reheating approximation itself (shown by black points). It is therefore possible to associate a signal significance of 5σ with MeV-scale reheating temperature and MeV-scale frozen in DM. This is what we depicted in the left panel of Fig. 1, via the white (cyan) dashed line(s).

An effective DM-electron interaction can also be realized at the 1-loop level [cf. right panel of Fig. 2], that leads to DM direct search via electron scattering, which is typically sensitive to MeV-scale DM [43]. However, in our case, corresponding scattering cross-section turns out to be $\lesssim 10^{-51}$ cm², far beyond the reach of present experiments [44–49].

To summarise, we propose that there is a possibility to infer the reheat temperature of the universe from collider signal of DM at future lepton colliders. The possibility emerges for DM components that undergo UV freeze-in, having one-to-one correspondence with T_{RH} , m_{DM} and NP scale Λ to address correct relic abundance. As a concrete example, we elucidate how the collider signature of an MeV scale photophilic fermionic DM can point towards MeV scale T_{RH} . Importantly, the mono- γ signal can be segregated from the SM background, when the photon emerges from the vertex, unlike the one from the ISR, which is typically overwhelmed with SM background. Here we only furnish the proof of the concept without getting involved into the details of the early Universe dynamics, or other types of DM operators, or signals which can provide similar inferences.

Acknowledgement: DP thanks the UGC for senior research fellowship. DP, SJ and AS would like to thank Cafe Coffee Day, IITG, where the inception of this idea took place. SB acknowledges WHEPP 2024 for discussion on low mass DM. We acknowledge use of TikzFeynman in generating the Feynman graphs.

-
- [1] N. Aghanim *et al.* (Planck), *Astron. Astrophys.* **641**, A6 (2020), [Erratum: *Astron.Astrophys.* 652, C4 (2021)], arXiv:1807.06209 [astro-ph.CO].
- [2] G. Jungman, M. Kamionkowski, and K. Griest, *Phys. Rept.* **267**, 195 (1996), arXiv:hep-ph/9506380.
- [3] L. J. Hall, K. Jedamzik, J. March-Russell, and S. M. West, *JHEP* **03**, 080 (2010), arXiv:0911.1120 [hep-ph].
- [4] F. Elahi, C. Kolda, and J. Unwin, *JHEP* **03**, 048 (2015), arXiv:1410.6157 [hep-ph].
- [5] J. Goodman, M. Ibe, A. Rajaraman, W. Shepherd, T. M. P. Tait, and H.-B. Yu, *Phys. Rev. D* **82**, 116010 (2010), arXiv:1008.1783 [hep-ph].
- [6] M. Beltran, D. Hooper, E. W. Kolb, and Z. C. Krusberg, *Phys. Rev. D* **80**, 043509 (2009), arXiv:0808.3384 [hep-ph].
- [7] Q.-H. Cao, C.-R. Chen, C. S. Li, and H. Zhang, *JHEP* **08**, 018 (2011), arXiv:0912.4511 [hep-ph].
- [8] M. A. Fedderke, J.-Y. Chen, E. W. Kolb, and L.-T. Wang, *JHEP* **08**, 122 (2014), arXiv:1404.2283 [hep-ph].
- [9] J.-H. Liang, Y. Liao, X.-D. Ma, and H.-L. Wang, *JHEP* **12**, 172 (2023), arXiv:2309.12166 [hep-ph].
- [10] T. Brauner, S. A. Hartnoll, P. Kovtun, H. Liu, M. Mezei, A. Nicolis, R. Penco, S.-H. Shao, and D. T. Son, in *Snowmass 2021* (2022) arXiv:2203.10110 [hep-th].
- [11] P. J. Fox, R. Harnik, J. Kopp, and Y. Tsai, *Phys. Rev. D* **84**, 014028 (2011), arXiv:1103.0240 [hep-ph].
- [12] Z.-H. Yu, Q.-S. Yan, and P.-F. Yin, *Phys. Rev. D* **88**, 075015 (2013), arXiv:1307.5740 [hep-ph].
- [13] R. Essig, J. Mardon, M. Papucci, T. Volansky, and Y.-M. Zhong, *JHEP* **11**, 167 (2013), arXiv:1309.5084 [hep-ph].
- [14] K. Kadota and J. Silk, *Phys. Rev. D* **89**, 103528 (2014), arXiv:1402.7295 [hep-ph].

- [15] Z.-H. Yu, X.-J. Bi, Q.-S. Yan, and P.-F. Yin, *Phys. Rev. D* **90**, 055010 (2014), arXiv:1404.6990 [hep-ph].
- [16] A. Freitas and S. Westhoff, *JHEP* **10**, 116 (2014), arXiv:1408.1959 [hep-ph].
- [17] S. Dutta, D. Sachdeva, and B. Rawat, *Eur. Phys. J. C* **77**, 639 (2017), arXiv:1704.03994 [hep-ph].
- [18] D. Choudhury and D. Sachdeva, *Phys. Rev. D* **100**, 075007 (2019), arXiv:1906.06364 [hep-ph].
- [19] S.-I. Horigome, T. Katayose, S. Matsumoto, and I. Saha, *Phys. Rev. D* **104**, 055001 (2021), arXiv:2102.08645 [hep-ph].
- [20] B. Barman, S. Bhattacharya, S. Girmohanta, and S. Jahedi, *JHEP* **04**, 146 (2022), arXiv:2109.10936 [hep-ph].
- [21] S. Kundu, A. Guha, P. K. Das, and P. S. B. Dev, *Phys. Rev. D* **107**, 015003 (2023), arXiv:2110.06903 [hep-ph].
- [22] S. Bhattacharya, P. Ghosh, J. Lahiri, and B. Mukhopadhyaya, *Phys. Rev. D* **108**, L111703 (2023), arXiv:2211.10749 [hep-ph].
- [23] S.-F. Ge, K. Ma, X.-D. Ma, and J. Sheng, *JHEP* **11**, 190 (2023), arXiv:2306.00657 [hep-ph].
- [24] K. Ma, *Chin. Phys. C* **46**, 113104 (2022), arXiv:2205.05560 [hep-ph].
- [25] A. Nelson, L. M. Carpenter, R. Cotta, A. Johnstone, and D. Whiteson, *Phys. Rev. D* **89**, 056011 (2014).
- [26] C. Arina, A. Cheek, K. Mimasu, and L. Pagani, *Eur. Phys. J. C* **81**, 223 (2021), arXiv:2005.12789 [hep-ph].
- [27] B. J. Kavanagh, P. Panci, and R. Ziegler, *JHEP* **04**, 089 (2019), arXiv:1810.00033 [hep-ph].
- [28] P. Gondolo and G. Gelmini, *Nucl. Phys. B* **360**, 145 (1991).
- [29] G. F. Giudice, E. W. Kolb, and A. Riotto, *Phys. Rev. D* **64**, 023508 (2001), arXiv:hep-ph/0005123.
- [30] R. L. Workman *et al.* (Particle Data Group), *PTEP* **2022**, 083C01 (2022).
- [31] K. Kaneta, Y. Mambrini, and K. A. Olive, *Phys. Rev. D* **99**, 063508 (2019), arXiv:1901.04449 [hep-ph].
- [32] B. Barman, N. Bernal, Y. Xu, and O. Zapata, *JCAP* **07**, 019 (2022), arXiv:2202.12906 [hep-ph].
- [33] S. Hannestad, *Phys. Rev. D* **70**, 043506 (2004), arXiv:astro-ph/0403291.
- [34] M. R. Haque and D. Maity, *Phys. Rev. D* **107**, 043531 (2023).
- [35] D. G. Figueroa and E. H. Tanin, *JCAP* **10**, 050 (2019), arXiv:1811.04093 [astro-ph.CO].
- [36] T. Opferkuch, P. Schwaller, and B. A. Stefanek, *JCAP* **07**, 016 (2019), arXiv:1905.06823 [gr-qc].
- [37] A. Aryshev *et al.* (ILC International Development Team), (2022), arXiv:2203.07622 [physics.acc-ph].
- [38] A. Alloul, N. D. Christensen, C. Degrande, C. Duhr, and B. Fuks, *Comput. Phys. Commun.* **185**, 2250 (2014), arXiv:1310.1921 [hep-ph].
- [39] J. Alwall, M. Herquet, F. Maltoni, O. Mattelaer, and T. Stelzer, *JHEP* **06**, 128 (2011), arXiv:1106.0522 [hep-ph].
- [40] T. Sjöstrand, S. Ask, J. R. Christiansen, R. Corke, N. Desai, P. Ilten, S. Mrenna, S. Prestel, C. O. Rasmussen, and P. Z. Skands, *Comput. Phys. Commun.* **191**, 159 (2015), arXiv:1410.3012 [hep-ph].
- [41] J. de Favereau, C. Delaere, P. Demin, A. Giammanco, V. Lemaitre, A. Mertens, and M. Selvaggi (DELPHES 3), *JHEP* **02**, 057 (2014), arXiv:1307.6346 [hep-ex].
- [42] G. Cowan, K. Cranmer, E. Gross, and O. Vitells, *Eur. Phys. J. C* **71**, 1554 (2011), [Erratum: *Eur.Phys.J.C* **73**, 2501 (2013)], arXiv:1007.1727 [physics.data-an].
- [43] R. Essig, J. Mardon, and T. Volansky, *Phys. Rev. D* **85**, 076007 (2012), arXiv:1108.5383 [hep-ph].
- [44] A. Aguilar-Arevalo *et al.* (DAMIC), *Phys. Rev. Lett.* **123**, 181802 (2019), arXiv:1907.12628 [astro-ph.CO].
- [45] L. Barak *et al.* (SENSEI), *Phys. Rev. Lett.* **125**, 171802 (2020), arXiv:2004.11378 [astro-ph.CO].
- [46] C. Cheng *et al.* (PandaX-II), *Phys. Rev. Lett.* **126**, 211803 (2021), arXiv:2101.07479 [hep-ex].
- [47] D. W. Amaral *et al.* (SuperCDMS), *Phys. Rev. D* **102**, 091101 (2020), arXiv:2005.14067 [hep-ex].
- [48] Z. Y. Zhang *et al.* (CDEX), *Phys. Rev. Lett.* **129**, 221301 (2022), arXiv:2206.04128 [hep-ex].
- [49] E. Aprile *et al.* (XENON), *Phys. Rev. Lett.* **131**, 041003 (2023), arXiv:2303.14729 [hep-ex].
- [50] J. Fuentes-Martín, M. König, J. Pagès, A. E. Thomsen, and F. Wilsch, *Eur. Phys. J. C* **83**, 662 (2023), arXiv:2212.04510 [hep-ph].

Supplemental Material

Appendix A: Radiation γ vs. Vertex γ

We review two scenarios in our analysis. The first scenario (already discussed in the main text) involves the operator \mathcal{O}_3^f , where the photon from the lepton collider mono- γ signal originates directly from the effective vertex itself. In the alternate scenario, the photon is radiated from the incoming electron/positron leg. The later scenario is relevant to DM produced via leptophilic operators. One such operator is given by

$$\mathcal{O}_2^f = \frac{c_\chi}{\Lambda^2} (\bar{\ell}_L \gamma^\mu \ell_L + \bar{e}_R \gamma^\mu e_R) (\bar{\chi} \gamma_\mu \chi). \quad (\text{A1})$$

We perform a comparative analysis between the vertex photon from \mathcal{O}_3^f and radiative photon from \mathcal{O}_2^f along with the neutrino background. The kinematic distributions are shown in Fig. 5. It can be clearly seen that the radiative process is always overshadowed by the SM neutrino background, and hence clear distinction is extremely difficult using cut-based methods. To segregate these signal processes, we require polarization tuning (to suppress the background) as well as dedicated multivariate techniques.

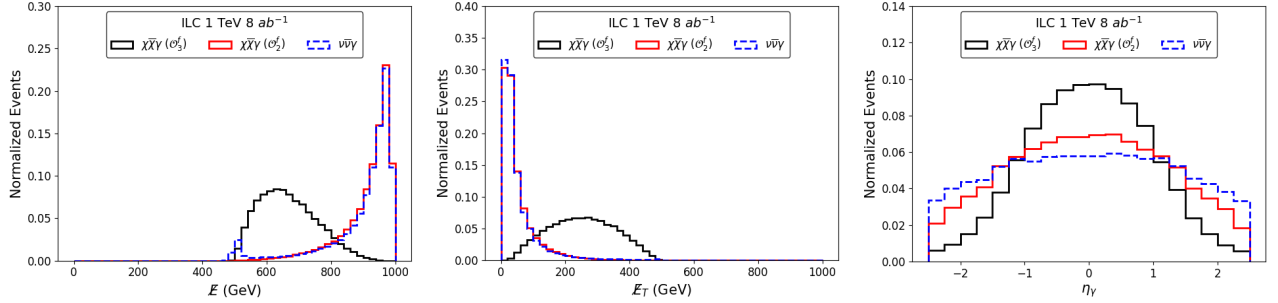


FIG. 5. Signal background event distributions for different kinematic variables with the mono- γ final state signal. Left: MET (E_T), middle: ME (E), right: Pseudorapidity (η_γ).

Appendix B: Reaction density and Boltzmann equation

The reaction density corresponding to 2-to-2 processes reads

$$\begin{aligned} \gamma_{22} &= \int \prod_{i=1}^4 d\Pi_i (2\pi)^4 \delta^{(4)}(p_a + p_b - p_1 - p_2) f_a^{\text{eq}} f_b^{\text{eq}} |\mathcal{M}_{a,b \rightarrow 1,2}|^2 \\ &= \frac{T}{32\pi^4} g_a g_b \int_{s_{\min}}^{\infty} ds \frac{\left[(s - m_a^2 - m_b^2)^2 - 4m_a^2 m_b^2 \right]}{\sqrt{s}} \sigma(s)_{a,b \rightarrow 1,2} K_1 \left(\frac{\sqrt{s}}{T} \right), \end{aligned} \quad (\text{B1})$$

with $a, b(1, 2)$ as the incoming (outgoing) states and $g_{a,b}$ are corresponding degrees of freedom. Here $f_i^{\text{eq}} \approx \exp^{-E_i/T}$ is the Maxwell-Boltzmann distribution. The Lorentz invariant 2-body phase space is denoted by: $d\Pi_i = \frac{d^3 p_i}{(2\pi)^3 2E_i}$. The amplitude squared (summed over final and averaged over initial states) is denoted by $|\mathcal{M}_{a,b \rightarrow 1,2}|^2$ for a particular 2-to-2 scattering process. The lower limit of the integration over s is $s_{\min} = \max \left[(m_a + m_b)^2, (m_1 + m_2)^2 \right]$.

The Boltzmann equation (BEQ) governing the DM number density can be written in terms of the DM yield defined as a ratio of the DM number density to the entropy density in the visible sector, i.e., $Y_{\text{DM}} = n_{\text{DM}}/s$. The BEQ can

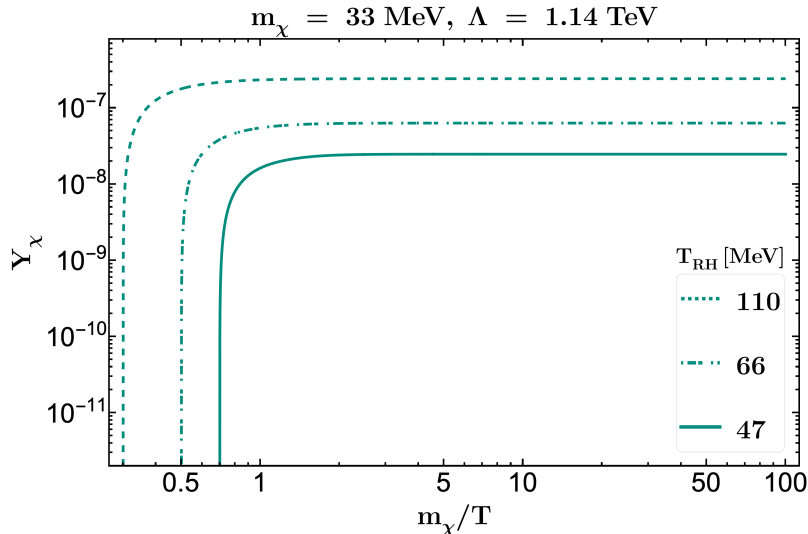


FIG. 6. Yield of fermionic DM as a function of the dimensionless quantity m_χ/T , where different curves correspond to different choices of $T_{\text{RH}} = \{47, 66, 110\}$ MeV, shown via solid, dot-dashed and dashed patterns, respectively. Here we have fixed $\Lambda = 1.14$ TeV and $m_\chi = 33$ MeV.

then be expressed in terms of the reaction densities as

$$x H s \frac{dY_{\text{DM}}}{dx} = \gamma_{22}, \quad (\text{B2})$$

where $x \equiv m_{\text{DM}}/T$, T being the temperature of the thermal bath and H is the Hubble parameter. In a radiation dominated Universe,

$$s(T) = \frac{2\pi^2}{45} g_{*s}(T) T^3, \quad H(T) = \frac{\pi}{3} \sqrt{\frac{g_*(T)}{10}} \frac{T^2}{M_P}, \quad (\text{B3})$$

where g_{*s} and g_* are the effective number of relativistic degrees of freedom contributing to the entropy and energy density respectively, while M_P is the reduced Planck mass. The typical UV nature of the DM yield is very much apparent from Fig. 6, where, as one can see, bulk of the DM production happens around T_{RH} , for a given DM mass and NP scale.

Appendix C: Possible UV-completion

We present possible UV completion scenarios for the operator \mathcal{O}_3^f as shown in Fig. 7. The \mathcal{O}_3^f matching requires inclusion of the following fields: a heavy vector-like (such that gauge anomaly cancellation within the SM remains unharmed) $SU(2)_L$ lepton doublet, Ψ with hypercharge $Y = \pm 1$, and a scalar doublet S with the same hypercharge as the lepton doublet, that connects to the SM through a Yukawa-type coupling with the lepton doublet, Ψ and the dark matter field χ . Here χ is odd under \mathbb{Z}_2 and either Ψ or S can be odd under \mathbb{Z}_2 while the other being even. The resulting UV-complete Lagrangian then reads,

$$\mathcal{L}_{\text{UV}} = \mathcal{L}_{\text{SM}} + \bar{\Psi}(i\gamma^\mu D_\mu - m_\Psi)\Psi + \bar{\chi}(i\gamma^\mu \partial_\mu - m_\chi)\chi + (D^\mu S)^\dagger (D_\mu S) - m_S^2 (S^\dagger S) - \mathcal{Y}_\chi (S^\dagger \bar{\chi} \Psi + S \bar{\Psi} \chi). \quad (\text{C1})$$

Here, $D_\mu = \partial_\mu - i\frac{g'}{2} Y B_\mu - i\frac{g}{2} \sigma^i W_\mu^i$ is $SU(2)_L \times U(1)_Y$ gauge covariant derivative. Performing a 1-loop matching of

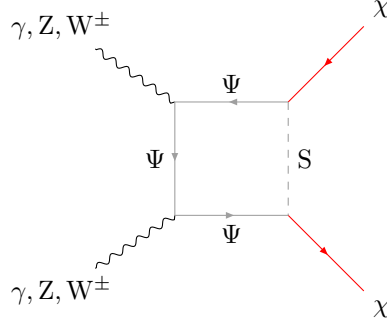


FIG. 7. Possible UV-completion for \mathcal{O}_3^f where χ (red lines) is our fermionic DM, Ψ and S (grey lines) are BSM particles relevant to our UV completion scenarios. The SM particles are represented by black lines.

this UV complete model with \mathcal{O}_3^f using `Matchete` [50], we obtain the relevant Wilson coefficients as

$$c_\chi = \frac{\mathcal{Y}_\chi^2 \Lambda^3}{24 m_S^3} \frac{x^6 - 6x^4 + 3x^2 + 2 + 12x^2 \log x}{(1-x^2)^3} \times \begin{cases} g^2 & \text{for } W_{\mu\nu}^i W^{i\mu\nu} \bar{\chi} \chi \\ (g')^2 & \text{for } B_{\mu\nu} B^{\mu\nu} \bar{\chi} \chi, \end{cases} \quad (\text{C2})$$

where $x = m_\Psi/m_S$.